Magnetic oxide formation at Al₂O₃/Co₈₄Fe₁₆ interface in magnetic tunnel junction

K.-J. Rho,[1] J.-S. Lee,[1,*] K.-B. Lee,[1] J.-H. Park,[1,2,†] J.-Y. Kim,[3] Y. J. Park,[3] K. J. Kim,[3] S. J. Joo,[4] and K. Rhie[4]

[1]*Department of Physics, Pohang University of Science and Technology, Pohang 790-784, Korea*
[2]*Division of Advanced Materials Science, Pohang University of Science and Technology, Pohang 790-784, Korea*
[3]*Pohang Accelerator Laboratory, Pohang University of Science and Technology, Pohang 790-784, Korea*
[4]*Department of Physics, Korea University, Chungnam 339-700, Korea*

We investigated the interfacial status of ferromagnetic Co₈₄Fe₁₆/insulating barrier Al₂O₃ of the Al₂O₃-based magnetic tunnel junction (MTJ) using various x-ray scattering measurements. The results show formation of orthorhombic AlFeO₃ magnetic nanoparticles at the interface, which are embedded in the Al₂O₃ cage. Their thickness and planner size vary with the plasma oxidation time. We also observed an interesting magnetic anomaly with a minimum magnetic coercivity near the AlFeO₃ ferrimagnetic T_C, which is successfully explained in terms of the AlFeO₃ nanoparticles and nanoscale CoFe grains with size distribution.

PACS number(s): 75.70.Cn, 78.70.Ck, 68.35.Ct, 81.40.Rs

Magnetic tunnel junctions (MTJs), which consist of two ferromagnetic layers separated by an insulating barrier and utilize the tunneling magnetoresistance (TMR), have attracted much attention due to their potential technological applications such as magnetic recording head, sensor, magnetic random access memory, etc.[1,2] The TMR value, the key functionality in MTJs, strongly varies with the quality and thickness of the insulating barrier.[3,4] Although recent observation of greatly enhanced TMR values in MgO-based MTJs somewhat takes over the application interests, the original Al₂O₃-based MTJ still retains interface related interesting physical phenomena such as anomalous temperature dependence and a Kondo-like behavior in the TMR value.[5–7] Furthermore, the interface problems are common issues in all MTJs since the TMR values can be affected seriously by the interface conditions. Various investigations have been attempted to understand the interfacial status, but none of them have ever directly provided full information on that due to technical difficulties.[8–11]

In this paper we explored the Al₂O₃/Co₈₄Fe₁₆ interface prepared with various post-oxidation times using the x-ray diffraction in conventional (XRD) and grazing incident (GIXRD) modes and the x-ray reflectivity (XRR). It was found that a magnetic oxide of orthorhombic AlFeO₃ phase is formed at the interface and its thickness varies with the oxidation time. The formed oxide was identified as pancake-like AlFeO₃ nanoparticles of several ten nanometer scale embedded in the Al₂O₃ cage. The magnetic coercivity exhibits an anomalous behavior with a broad minimum near a certain temperature, which is close to the magnetic ordering temperature $T_C \sim$ 250 K of bulk AlFeO₃, and the minimum temperature shifts with the oxidation time. Interestingly, the similar behaviors can be also observable in the TMR value, indicating the importance of the interface effect in the tunneling mechanism. The coercivity increases as temperature increases above the minimum temperature due to formation of nanoscale CoFe grains with size distribution.

Polycrystalline films with a simplified structure Al₂O₃/Co₈₄Fe₁₆(30Å)/Ta(120Å)/SiO₂/Si were fabricated under a 200 Oe magnetic field for uniaxial magnetic anisotropy by using the dc magnetron sputtering. The Al₂O₃ layer was formed by post plasma oxidation of an Al

($\sim$10Å) layer with oxidation time t_o = 4, 8, 12, 16, 20, and 28 s, followed by a 25 s rapid annealing at $T = 300\,°$C as in the growth of the MTJs.[7,12] XRD and XRR results were collected by using 4-circle diffractometer with photon energy 8.05 keV as in the Cu $K\alpha$ line at the 3C2 beamline in Pohang Light Source (PLS). Conventional XRD data were obtained in specular condition ($\theta = 2\theta/2$). In GIXRD the incident angle is fixed at an angle as low as $\alpha \sim 0.5°$ to optimize the surface sensitivity.[13] The real space image of the surface/interface morphology was obtained by using the scanning electron microscopy (SEM) and transmission electron microscopy (TEM), and MOKE measurements were carried out for the magnetic hysteresis behaviors at various temperatures.

Figure 1(a) shows conventional XRD patterns of the films with different t_o, all which display three noticeable peaks of Ta (002), Al₂O₃ (110), and CoFe (110). We also performed the surface sensitive GIXRD measurements at a minimal incident angle ($\alpha \sim 0.5°$). As shown in Fig. 1(b), even the remarkable CoFe (110) peak almost disappears, and the contribution from the underneath Ta is not expected. Hence the result is considered as contributions from the surface/interface region. Differently from XRD, GIXRD exhibits two major peaks **A** and **B** denoted in Fig. 1. As t_o increases, peak **A**, which is negligible in the naturally oxidized as-grown sample without the plasma oxidation and annealing processes, grows up and peak **B** becomes sharper. For $t_o \geqslant 12$ s the variation becomes minimal. The XRD and GIXRD results of the $t_o = 12$ s film are compared in Fig. 1(c). Peak **B** is assigned to Al₂O₃ (110) from the coincident peak position. Its broad peak shape in the as-grown sample is attributed to the amorphous AlO$_x$.

Peak **A** is unexpected in the desired Al₂O₃/CoFe/Ta film structure, indicating formation of an additional oxide in the interfacial region. Its position is slightly different from that of Ta (002). One may imagine possible formation of Al and CoFe intermixed oxide at the interface during the oxidation process. We checked XRD patterns of all possible candidates of the Al-Co-Fe-O composition and could identify peak **A** as the (122) Bragg peak of orthorhombic AlFeO₃, which is a ferrimagnet with $T_C \simeq 250$ K.[14] As can be seen in Fig. 1, the peak **A** position exactly matches the AlFeO₃ (122) peak with the highest intensity.[15] Besides the main (122) peak, other
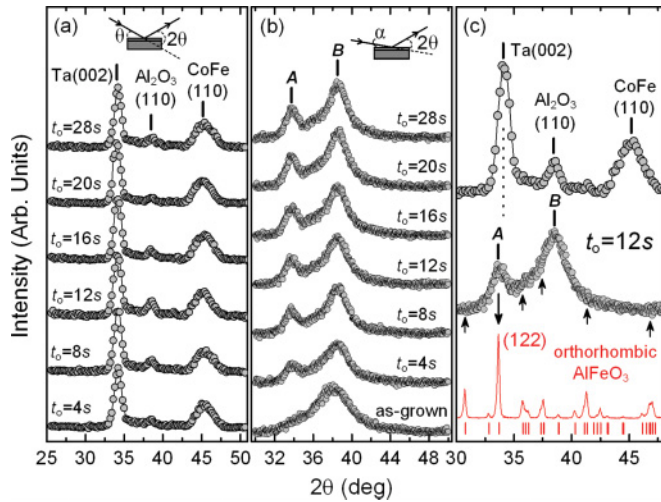
FIG. 1. (Color online) (a) Conventional XRD and (b) GIXRD patterns of the films of different t_o. Vertical lines indicate *hkl* Bragg peak positions of Ta, Al_2O_3, and CoFe. Their experimental configurations are presented schematically. (c) XRD and GIXRD results of the $t_o = 12$ s film compared with the reference XRD pattern of $AlFeO_3$.[15]

minor peaks are partly observable in the GIXRD, although those are obscured by the experimental noise of the intensive Al_2O_3 (110) peak.

We investigated the layered structure of the films using XRR. Figure 2(a) shows the results for the films of $t_o = 4, 8, 12,$ and 28 s. The XRR clearly display intensity oscillations, the so-called Kiessig oscillations,[13] for all the films, resulting from interference of reflected lights at different interfaces. The oscillation period and XRR curve slope reflect the layer thickness and film roughness, respectively. The smallest oscillation period and the curve slope are nearly identical for all the films, meaning that the respective total thickness and overall roughness barely vary with t_o. We found, however,
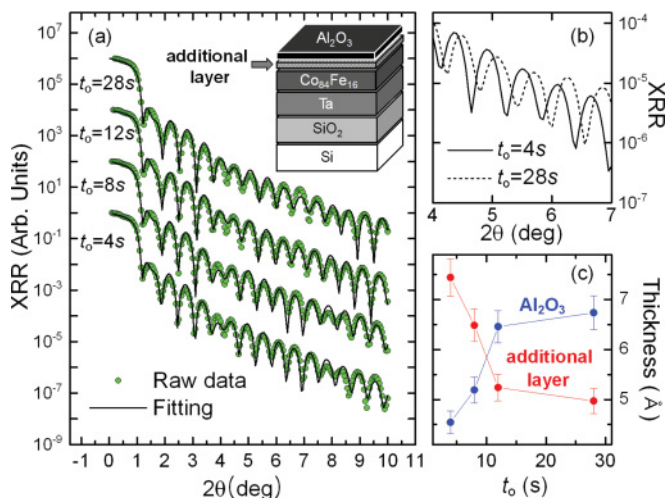
FIG. 2. (Color online) (a) XRR data (circles) and their fits (lines) for films with different t_o. Inset shows model structure for fitting. (b) Magnified XRR data of the $t_o = 4$ and 28 s films. (c) Thicknesses of the Al_2O_3 and additional layers obtained from fitting parameters.

a clear difference in the oscillation phase for samples with different t_o as shown in direct comparison of the magnified curves for $t_o = 4$ and 28 s in Fig. 2(b). Such phase difference tells us that there are certain differences in the electron density and thickness of each layer without a significant change in the total thickness or roughness.

For the quantitative information, we fitted the XRR results using a general recursive equation based on Parratt formula.[16] It should be noted that in the original Al_2O_3/CoFe/Ta/SiO_2/Si structure, the theoretical fit does not reproduce properly the data even with all possible parameter sets of roughnesses, thicknesses, and electron densities. Meanwhile, when an additional layer, which has the electron density different from that of Al_2O_3 layer, is introduced between Al_2O_3 and CoFe layers [see the inset in Fig. 2(a)], the calculated XRR agrees well with the measured one. The electron density used in the fit, which monotonically increases with the oxidation time, ranges from 11.88×10^{23} to $12.34 \times 10^{23}/cm^3$, which is larger than the density of Al_2O_3 ($11.78 \times 10^{23}/cm^3$) but smaller than that of $AlFeO_3$ ($12.7513 \times 10^{23}/cm^3$), indicating that the additional layer is a sort of a mixture of Al_2O_3 and $AlFeO_3$. The fit estimates the total thickness of 178 Å and the average roughness of 3 Å for all the samples. The roughness was applied in the fit in a standard way through the height variation with a Gaussian distribution, and the average roughness is taken from the root-mean-square value of the variation.[17–19] The phase differences are reproduced by applying different thicknesses for both the Al_2O_3 layer and the additional layer together with the electron density variation of the additional layer. Figure 2(c) presents the thicknesses determined from the fit. Al_2O_3 thickness increases but the additional layer thickness decreases as t_o increases with keeping the sum nearly fixed at ~12 Å.

In order to examine how $AlFeO_3$ is mixed with Al_2O_3 in the additional layer, we checked the surface and interface morphology using the SEM and TEM measurements. Considering that the probing depth of the SEM is about 100 Å, the image reflects not only the surface but also the interface.[20] Figures 3(a) and 3(b) show the SEM images for the $t_o = 8$ and 12 s samples, which show nanosized $AlFeO_3$ particles randomly distributed. The $AlFeO_3$ is more conducting at room temperature than Al_2O_3 and exhibits brighter images in SEM. One can recognize $AlFeO_3$ nanoparticles with diameters of several ten nanometers in both images, and the overall size of the particles increases for the $t_o = 12$ s sample. The $AlFeO_3$ nanoparticles can be also observable in the cross-sectional TEM image of the $t_o = 12$ s film presented in Fig. 3(c). The wide range TEM image clearly shows the pancake-like $AlFeO_3$ nanoparticles at the interface with the lateral size of roughly 20–50 nm and the thicknesses less than 1 nm. From these results, we confidently conclude that the pancake-like $AlFeO_3$ nanoparticles are formed at the interface during the oxidation process. One can also notice that the additional layer in the XRR studies corresponds to a mixed layer of the pancake-like $AlFeO_3$ nanoparticles in the Al_2O_3 cages, rather than an entire homogeneous $AlFeO_3$ layer. In addition, the GIXRD and XRR results, increases of both $AlFeO_3$ (122) peak intensity and the electron density of the additional layer but decrease of the layer thickness, are also consistent with the microscopic observation that the $AlFeO_3$
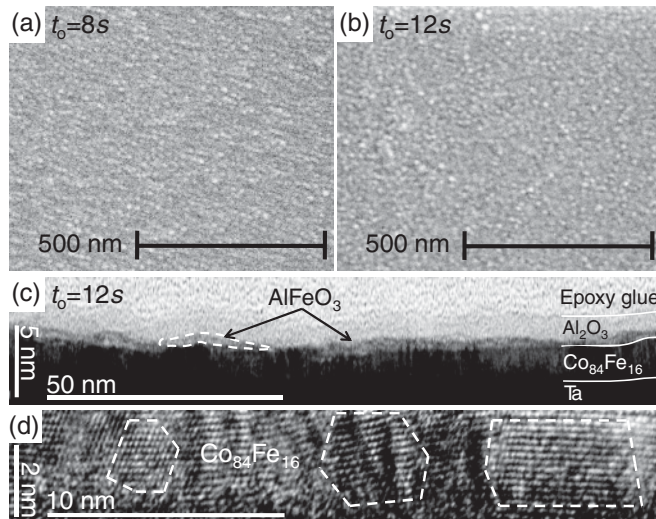
FIG. 3. SEM images of the films of (a) $t_o = 8$ s and (b) 12 s. (c) Wide range HRTEM image for epoxy/Al_2O_3($AlFeO_3$)/CoFe/Ta in the $t_o = 12$ s film. $AlFeO_3$ nanoparticles with 20–50 nm lateral size are embedded in the Al_2O_3 layer. As an example, a 20 nm nanoparticle is presented with a close white dashed line. (d) Enlarged HRTEM image of $Co_{84}Fe_{16}$ layer in the film, which shows the nanoscale grains. Some of the grains are presented with close white dashed lines.

particles become flatter as t_o increases, that is, the larger planner size but the smaller thickness. On the other hand, we also observed formation of the ferromagnetic $Co_{84}Fe_{16}$ grains with size distribution in 2–10 nm in the high-resolution TEM image as presented in Fig. 3(d). The formed nanoscale CoFe ferromagnetic grains with the size distribution exhibit an abnormal behavior in the magnetic coercivity as discussed below.

The $AlFeO_3$ magnetic nanoparticles likely interact with the underlying CoFe ferromagentic layer to affect its magnetic property. Figure 4(a) shows magnetic hysteresis curves of the $t_o = 8$ s film at various temperatures obtained from the MOKE measurements. Coercive field H_C strongly varies with temperature with a minimum $H_C \simeq 20$ Oe at $T_{min} \sim 200$ K. Figure 4(b) displays the temperature dependence of coercivity for the samples of $t_o = 4$, 8, and 12 s, which all show the anomalous behavior with T_{min}. In the $t_o = 4$ s sample where the additional layer has the largest average thickness of about two $AlFeO_3$ formula unit cell, we observed $T_{min} \simeq 230$ K, which is close to $T_C \simeq 250$ K of bulk $AlFeO_3$. It implies that the magnetic ordering of the $AlFeO_3$ nanoparticles at the interface is responsible for the behavior. As observed previously in ferromagnet systems interfacing magnetic oxide nanoparticles, the rapid increase of H_C upon cooling below T_{min} can be understood in terms of the interfacial exchange interaction.[21,22] On the other hand, the enhancement of H_C upon heating above T_{min} is attributed to the nanoscale CoFe grains with size distribution as shown in Fig. 3(d). The nanoscale CoFe grain with a few nanometer size, which shows superparamagnetism above the blocking temperature T_B, is expected to have T_B even below 100 K as observed in FePt nanoparticles,[23] and T_B increases as the grain size increases. Therefore, as temperature T increases, the
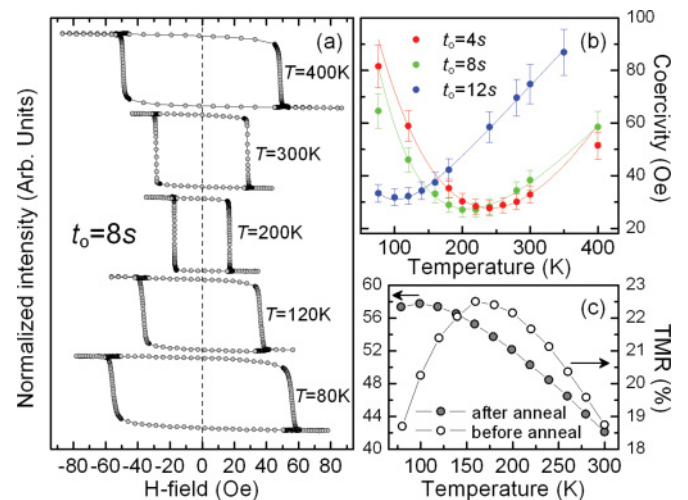
more CoFe grains with $T_B < T$ become supermaramagnetic and H_C becomes larger until T reaches T_B of the large grains, as observed previously in other ferromagentic granular systems.[24,25]

T_{min} becomes reduced to $T_{min} \simeq 200$ K for $t_o = 8$ s and $T_{min} \simeq 100$ K for $t_o = 12$ s, and then does not change much for $t_o > 12$ s.[15] The decrease of T_{min} is consistent with the decrease of the $AlFeO_3$ nanoparticle thickness observed in the XRR results. The ordering temperature in magnetic systems is generally reduced with decrease of the thickness in a few unit cell range,[26,27] although the thickness dependence of T_C in $AlFeO_3$ is unknown. Interestingly, as presented in Fig. 4(c), the TMR value of MTJ ($Co_{84}Fe_{16}$/Al_2O_3/$Co_{84}Fe_{16}$) also showed the similar tendencies before and after annealing[7] as the observed temperature dependence and shift of T_{min} in our films; the TMR shows an anomalous temperature dependent behavior with a maximum value at a certain temperature T_{max}, and T_{max} shifts from 150 to 100 K after annealing. The situation may not be the same, but our findings are meaningful to understand this awkward temperature dependent behavior of the TMR value in the Al_2O_3/CoFe-based MTJs, which were fabricated in the same processes. The annealing process, which improves the transport properties,[7,12] generally reduces not only intermixing of the insulating barrier and the ferromagnetic layer but also the layer roughness. Thus this similarity indicates that the $AlFeO_3$ nanoparticles, which can be expected to form at the interface, also becomes flatter through annealing process and then its magnetic ordering temperature is reduced, at which magnetic scattering is turned on and the TMR value is suppressed upon cooling.

In summary, we made a detailed structural investigation on the Al_2O_3/CoFe interfacial region in the Al_2O_3-based MTJ system. We found that an additional oxide layer with $AlFeO_3$ magnetic nanoparticles in the Al_2O_3 cages is formed at the interface in the fabrication process and that the nanoparticles affect not only the magnetic properties but also the TMR value of the corresponding MTJ.

FIG. 4. (Color online) (a) Magnetic hysteresis curves of the $t_o = 8$ s film. (b) Temperature dependence of coercivity for the $t_o = 4$, 8, and 12 s films. The solid lines are a guide for the eye. (c) Temperature dependence of TMR of MTJ before and after annealing taken from Ref. 7.

---

[*]Present address: SSRL, SLAC National Accelerator Laboratory, Menlo Park, CA 94025, USA.

[†]Correspondence should be addressed to jhp@postech.ac.kr

[1]G. A. Prinz, Science **282**, 1660 (1998).

[2]S. A. Wolf, D. D. Awschalom, R. A. Buhrman, J. M. Daughton, S. von Molnar, M. L. Roukes, A. Y. Chtchelkanova, and D. Treger, Science **294**, 1488 (2001).

[3]J. M. Moodera, E. F. Gallagher, K. Robinson, and J. Nowak, Appl. Phys. Lett. **70**, 3050 (1997).

[4]M. Covington, J. Nowak, and D. Song, Appl. Phys. Lett. **76**, 3965 (2000).

[5]K. W. Kim, J. H. Koo, I. J. Shin, J. S. Kwak, J. P. Hong, and S. J. Woo, IEEE Trans. Magn. **45**, 60 (2009).

[6]K. I. Lee, S. J. Joo, J. H. Lee, K. Rhie, T.-S. Kim, W. Y. Lee, K. H. Shin, B. C. Lee, P. LeClair, J.-S. Lee, and J.-H. Park, Phys. Rev. Lett. **98**, 107202 (2007).

[7]J. H. Lee, I.-W. Chang, S. J. Byun, K. Rhie, K.-H. Shin, K. I. Lee, J. G. Ha, and B. C. Lee, J. Magn. Magn. Mater. **240**, 149 (2002).

[8]D. Lee and J. Hong, J. Appl. Phys. **97**, 093905 (2005).

[9]H.-J. Lee, S.-Y. Jeong, C. R. Cho, J. H. Lee, S. J. Joo, K. H. Shin, B. C. Lee, T.-S. Kim, J.-H. Park, J.-S. Kang, and K. Rhie, J. Appl. Phys. **97**, 033906 (2005).

[10]K. S. Yoon, J. Y. Yang, W. J. Choi, C. O. Kim, J. P. Hong, and H. J. Kim, Phys. Rev. B **69**, 012407 (2004).

[11]H. Schmitt, M. Ghafari, R. Kruk, J. Ellrich, A. Hütten, L. A. Schmitt, and H. Hahn, Appl. Phys. Lett. **88**, 122505 (2006).

[12]K. I. Lee, J. H. Lee, W. Y. Lee, K. W. Rhie, J. G. Ha, C. S. Kim, and K. H. Shin, J. Magn. Magn. Mater. **239**, 120 (2002).

[13]M. Birkholz, *Thin Film Analysis by X-ray Scattering* (Wiley, Weinheim, 2006).

[14]F. Bouree, J. L. Baudour, E. Elbadraoui, J. Musso, C. Laurent, and A. Rousset, Acta Crystallogr. Sect. B **52**, 217 (1996).

[15]K.-J. Rho *et al.* (unpublished).

[16]L. G. Parratt, Phys. Rev. **95**, 359 (1954).

[17]J. Als-Nielsen and D. McMorrow, *Elements of Modern X-ray Physics* (Wiley, West Sussex, UK, 2001).

[18]W. F. Egelhoff Jr., P. J. Chen, R. D. McMichael, C. J. Powell, R. D. Deslattes, F. G. Serpa, and R. D. Gomez, J. Appl. Phys. **89**, 5209 (2001).

[19]Yun Li and Shan X. Wang, J. Appl. Phys. **91**, 7950 (2002).

[20]J. Goldstein, D. E. Newbury, D. C. Joy, C. E. Lyman, P. Echlin, E. Lifshin, L. Sawyer, and J. R. Michael, *Scanning Electron Microscopy and X-ray Microanalysis* (Kluwer Academic, New York, 2003).

[21]E. Fulcomer and S. H. Charap, J. Appl. Phys. **43**, 4190 (1972).

[22]C. Leighton, J. Nogues, and B. J. Jönsson-Åkerman, and I. K. Schuller, Phys. Rev. Lett. **84**, 3466 (2000).

[23]B. Rellinghaus, S. Stappert, M. Acet, and E. F. Wassermann, J. Magn. Magn. Mater. **266**, 142 (2003).

[24]W. C. Nunes, W. S. D. Folly, J. P. Sinnecker, and M. A. Novak, Phys. Rev. B **70**, 014419 (2004).

[25]A. M. Zeltser and W. A. Soffa, J. Appl. Phys. **67**, 6958 (1990).

[26]T. Ambrose and C. L. Chien, J. Appl. Phys. **83**, 6822 (1998).

[27]P. J. van der Zaag, Y. Ijiri, J. A. Borchers, L. F. Feiner, R. M. Wolf, J. M. Gaines, R. W. Erwin, and M. A. Verheijen, Phys. Rev. Lett. **84**, 6102 (2000).